Genetic disruption of the small GTPase RAC1 prevents plexiform neurofibroma formation in mice with neurofibromatosis type 1

Received for publication, September 10, 2019, and in revised form, May 27, 2020 Published, Papers in Press, May 29, 2020, DOI 10.1074/jbc.RA119.010981

Julie A. Mund[1,2], SuJung Park[1], Abbi E. Smith[1], Yongzheng He[1], Li Jiang[1], Eric Hawley[1,2], Michelle J. Roberson[1], Dana K. Mitchell[1], Mohannad Abu-Sultanah[1], Jin Yuan[1], Waylan K. Bessler[1], George Sandusky[4], Shi Chen[1], Chi Zhang[3], Steven D. Rhodes[1,5], and D. Wade Clapp[1,2,3,*]

From the [1]Department of Pediatrics, Herman B. Wells Center for Pediatric Research, the Departments of [2]Biochemistry and Molecular Biology, [3]Medical and Molecular Genetics, the [4]Division of Pediatric Hematology–Oncology, and the [5]Department of Pathology, Indiana University School of Medicine, Indianapolis, Indiana, USA

Edited by Eric R. Fearon

Neurofibromatosis type 1 (NF1) is a common cancer predisposition syndrome caused by mutations in the *NF1* tumor suppressor gene. *NF1* encodes neurofibromin, a GTPase-activating protein for RAS proto-oncogene GTPase (RAS). Plexiform neurofibromas are a hallmark of NF1 and result from loss of heterozygosity of *NF1* in Schwann cells, leading to constitutively activated p21RAS. Given the inability to target p21RAS directly, here we performed an shRNA library screen of all human kinases and Rho-GTPases in a patient-derived $NF1^{-/-}$ Schwann cell line to identify novel therapeutic targets to disrupt PN formation and progression. Rho family members, including Rac family small GTPase 1 (RAC1), were identified as candidates. Corroborating these findings, we observed that shRNA-mediated knockdown of RAC1 reduces cell proliferation and phosphorylation of extracellular signal–regulated kinase (ERK) in $NF1^{-/-}$ Schwann cells. Genetically engineered $Nf1^{flox/flox}$;$PostnCre^{+}$ mice, which develop multiple PNs, also exhibited increased RAC1-GTP and phospho-ERK levels compared with $Nf1^{flox/flox}$;$PostnCre^{-}$ littermates. Notably, mice in which both *Nf1* and *Rac1* loci were disrupted ($Nf1^{flox/flox}Rac1^{flox/flox}$;$PostnCre^{+}$) were completely free of tumors and had normal phospho-ERK activity compared with $Nf1^{flox/flox}$;$PostnCre^{+}$ mice. We conclude that the RAC1-GTPase is a key downstream node of RAS and that genetic disruption of the *Rac1* allele completely prevents PN tumor formation *in vivo* in mice.

Neurofibromatosis type 1 (NF1) is an autosomal dominant disease affecting ~1 of 3500 individuals with ~50% of patients acquiring a *de novo* mutation. Mutations in the *NF1* tumor suppressor gene leads to constitutively active RAS, a binary molecular switch, through loss of the RAS–GTPase-activating protein (GAP), neurofibromin (1, 2). NF1 patients are heterozygous for *NF1*, but loss of heterozygosity of *NF1* in Schwann cells leads to complete loss of protein expression and drives the development of cutaneous and plexiform neurofibromas (PNs). Neurofibromin is a large protein, over 2800 amino acids; however, the GAP-related domain (GRD) is only ~300 amino acids and its reintroduction is sufficient to restore RAS activation, proliferation, and cytokine signaling in *NF1/Nf1* Null cells (3–5). Hyperactive RAS leads to increased RAS–RAF–MEK–ERK signaling driving aberrant cellular proliferation (6, 7). Efforts to target RAS directly have largely failed because of its many post-translational modifications and the relatively small size of the binding pocket for putative therapeutics (8). Inherent redundancies and feedback loops in RAS effector pathways have further confounded its direct targeting through small molecule inhibitors. In NF1 patients, dysregulation of the RAS–GAP molecular switch drives many comorbidities, including Schwann cell–derived PN. PN contain fibroblasts, endothelial cells, perineural cells, and infiltrating immune cells (9). These nonmalignant tumors collectively affect up to 40% of NF1 patients. The tumors are unresponsive to traditional chemotherapy (10). Surgical resection is often not possible and frequently involves major lifelong morbidity because the tumors arise from large peripheral nerves (11). Thus, novel targets are needed to develop or repurpose compounds for the treatment of PN.

Kinases have provided tractable therapeutic candidates in many human cancers and have provided the first effective targeted therapies for plexiform neurofibromas in NF1 (12, 13). There is known cross-talk between Rho-GTPases, which are members of the RAS superfamily, in both *Nf1*-deficient and other hyperactive RAS-mediated pathways (14, 15). Additionally, Rho GTPases have critical roles in many cellular functions including migration, cell adhesion, motility, proliferation, survival, and actin cytoskeleton organization and are increasingly recognized for their role in cancer, including metastasis and drug resistance (15–25). To identify critical and potentially druggable RAS effectors in the context of *NF1* loss, we performed a shRNA library screen containing all human kinases and Rho-GTPases. The screen identified RAS-related C3 botulinum toxin substrate 1 (RAC1) as preferentially reducing the growth of human *NF1* nullizygous Schwann cells. Genetic proof-of-concept studies further demonstrated an indispensable role for RAC1 in PN formation both *in vitro* and *in vivo* using genetically intercrossed mice in disease relevant tissues and cells. Collectively, these studies demonstrate that genetic disruption of RAC1 in tumorigenic $NF1^{-/-}$ Schwann cells restores ERK1/2 activation and proliferation *in vitro* and prevents PN formation in an established disease model.

This article contains supporting information.

* For correspondence: D. Wade Clapp, dclapp@iu.edu.

Results

Insertion of the NF1 GAP-related domain decreases RAS activity and proliferation in NF1$^{-/-}$ immortalized human Schwann cells

A patient-derived 05.5 *NF1*$^{-/-}$ immortalized Schwann cell line previously characterized to have hyperactive proliferation and increased ERK phosphorylation in response to serum was utilized (26). To reduce variability between *NF1*-deficient and competent cell lines, we created an isogenic cell pair. Using the previously published GRD sequence, a lentiviral construct containing both the GRD and a GFP reporter was generated (Fig. S1, *A* and *B*) (3, 4). Additionally, a scramble shRNA construct with a GFP reporter was also generated to ensure purified populations of transduced cells. Following transduction with each respective construct, the cells were sorted via FACS by GFP fluorescence, and the cell lines were expanded. The cell lines were termed Null (*NF1*$^{-/-}$) and GRD (expressing the human GRD transgene). The GRD was detected in protein lysates with and without the proteasome inhibitor MG-132 in the GRD-transduced cell line only. No GRD was detected in the Null lysates with or without MG-132 treatment (Fig. S1*C*). The activity of the GRD insert was then verified in functional and biochemical assays. RAS activation immunoprecipitation (IP) assays were performed to capture the RAF-1 RAS-binding domain. Only active RAS binds to the RAF-1 RAS-binding domain agarose bead, thus allowing RAS-GTP to be selected from protein lysates. As expected, the GRD protein lysates had decreased GTP-bound RAS compared with the Null protein lysates consistent with amelioration of RAS hyperactivation (Fig. 1*A*). GRD correction also decreased RAS effector signaling via the RAS–RAF–MEK cascade as shown by reduction in phospho-ERK1/2 signaling in GRD cells compared with the Null (Fig. 1*B*). Finally, GRD cells had decreased proliferation at both 48- and 72-h time points compared with Null cells (Fig. 1*C*).

A functional genomic screen identifies RAC1 as a key mediator of NF1$^{-/-}$ Schwann cell growth

A kinome and Rho-GTPase wide shRNA library screen was conducted to identify signaling networks essential to the growth of *NF1*$^{-/-}$ Schwann cells (Fig. 2*A*). Multiple clones per gene, based on prior work (27), were chosen because transduction efficiency varies from construct to construct. The combined shRNA library includes 3200 shRNA hairpins targeting 501 genes. A list of the clones used in the Rho-GTPase screen and the shRNA sequencing read counts for each clone and biological replicate are provided in Tables S1 and S2. Pathway analysis revealed enrichment of Rho GTPase family members, including those involved in Rho cell motility signaling, PTEN signaling, RAS signaling, MAL (MyD88 adapter-like) in Rho-mediated activation of SRC, RAC1 cell motility signaling, and PI3K subunit p85 in regulation of actin organization and cell migration. The identified PTEN, RAS, MAL, RAC1, and PI3K signatures all contained RAC1 (shRNA log fold change = −6.3 in *NF1*$^{-/-}$ cells *versus* GRD) as a candidate, as well as other related genes such as RHOA. RAC1 is also intricately linked to PI3K and RAF/MEK/ERK signaling. STRING analysis verified these effectors as exhibiting known and/or predicted protein interactions with RAC1 (Fig. 2*C*). Collectively, these data suggested that suppression of *RAC1* would abrogate gain-in-functions in *NF1*$^{-/-}$ Schwann cells mediated through hyperactive RAS signaling.

RAC1 knockdown in NF1$^{-/-}$ immortalized human Schwann cells reduces proliferation and phospho-ERK1/2 signaling

To evaluate the role of RAC1 in modulating RAS signaling in *NF1*$^{-/-}$ (Null) Schwann cells, a lentiviral construct was utilized to silence RAC1. Following transduction and puromycin selection, proliferation and Western blotting assays were performed. Protein lysates in the Null + RAC1 shRNA-treated cells had significantly less phospho-ERK1/2 signaling at both 15 and 30 min after stimulation compared with the Null cell lysates (Fig. 2*D*). Proliferation experiments were performed to compare the Null, GRD, and Null + RAC1 shRNA cell lines. At 48 h, proliferation was decreased in the Null + RAC1 shRNA cells compared with the Null cells (Fig. 2*E*). Additionally, GRD cells proliferated more slowly than both the Null and Null + RAC1 shRNA cells (Fig. 2*E*). At 72 h, both the GRD and Null + RAC1 shRNA cells were significantly decreased compared with the Null cells (Fig. 2*E*). As a complementary approach, Null and GRD cells were treated with the RAC1 inhibitor, EHop-016, for 24 and 48 h. EHop-016–treated cells also showed decreased proliferation (Fig. S2). Thus, loss of RAC1 in *NF1*$^{-/-}$ Schwann cells has functional consequences in both proliferation and phospho-ERK1/2 signaling, validating its potential as a target for PN amelioration.

Loss of Rac1 ameliorates gains in function within the plexiform neurofibroma tumorigenic cell of origin

We next determined whether RAC1-GTP was increased in the nerve tissues of genetically engineered *Nf1*$^{flox/flox}$;*PostnCre*$^{+}$ mice, which recapitulate human PNs in both development and histology (28). GTP-bound RAC1 was immunoprecipitated from trigeminal nerve tissues of *Nf1*$^{flox/flox}$;*PostnCre*$^{+}$ (*Nf1*$^{-/-}$) and *Nf1*$^{flox/flox}$;*PostnCre*$^{-}$ (WT). *Nf1*$^{-/-}$ mice exhibited significantly increased levels of RAC1-GTP (Fig. 3*A*).

A population of dorsal root ganglion/nerve root neurosphere cells (DNSCs) have been shown to contain the tumorigenic cell for PN in mice (28, 29). We isolated and expanded DNSCs from *Nf1*$^{flox/flox}$ and *Nf1*$^{flox/flox}$;*Rac1*$^{flox/flox}$ embryonic day 13.5 (E13.5) embryos generated by genetic intercross. Genetic ablation of floxed *Nf1* and *Rac1* alleles was achieved *ex vivo* via transient infection with Cre-GFP or GFP reporter adenovirus, yielding three resulting genotypes of DNSCs: WT, *Nf1*$^{-/-}$, and *Nf1*$^{-/-}$;*Rac1*$^{-/-}$ (DKO). Recombination of *Nf1* and *Rac1* was verified by PCR (Fig. 3*B*). Western blotting assays verified the loss of both neurofibromin and RAC1 in the cells treated with the Cre-GFP adenovirus (Fig. 3*B*). *Nf1*$^{-/-}$ DNSCs had hyperactive phospho-ERK1/2 (pERK1/2) at baseline and following stimulation compared with WT cells (Fig. 3*B*). Notably, the pERK1/2 levels in DKO DNSCs were significantly reduced following the 15-min stimulation with serum and were comparable with the WT (Fig. 3*C*). Phospho-AKT protein levels were also elevated at baseline following overnight starvation in the *Nf1*$^{-/-}$ DNSCs compared with WT and DKO DNSCs (Fig. 3*C*).

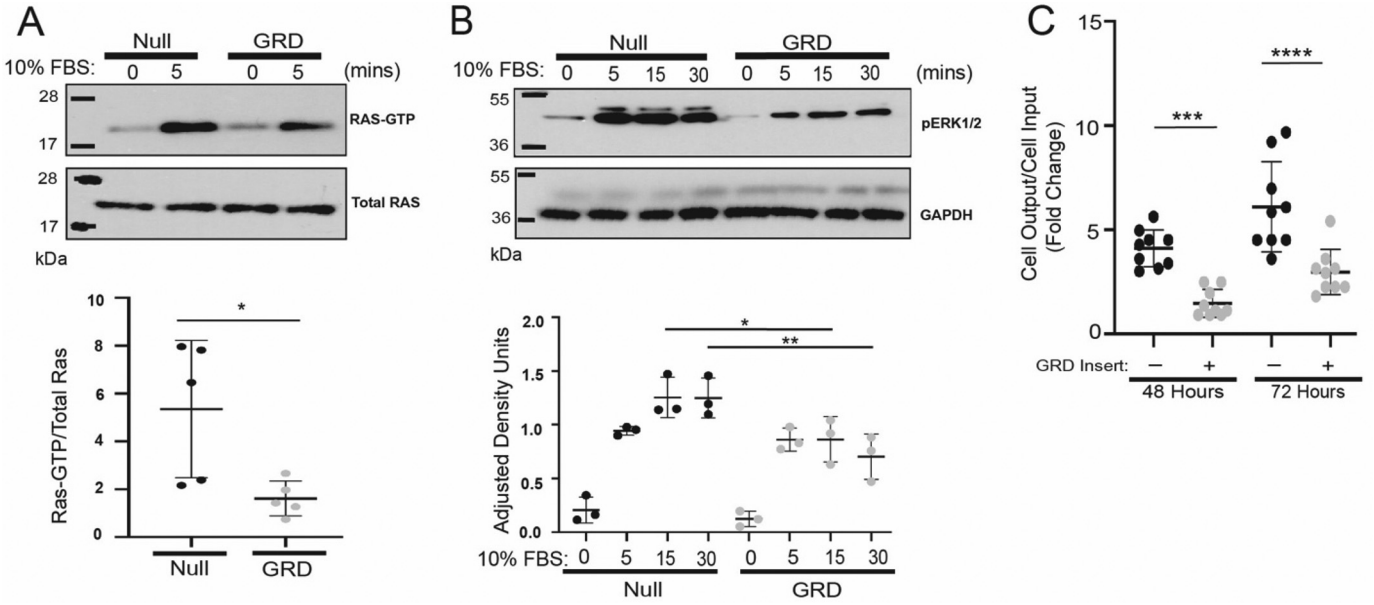

Figure 1. Insertion of the GRD of NF1 into patient-derived *NF1*$^{-/-}$ (Null) Schwann cells for use in a full human kinase and Rho-GTPase shRNA library screen. *A*, lentiviral insertion of the GRD of NF1 decreases RAS-GTP levels as compared with *NF1*$^{-/-}$ Schwann cells (Null) transduced with a scramble nontargeting GFP shRNA construct following stimulation with 10% FBS in DMEM. *, $p < 0.05$. *B*, hyperactive phospho-ERK1/2 signaling is attenuated at 15 and 30 min after stimulation with 10% FBS in DMEM in GRD compared with Null cells. *, $p < 0.05$; **, $p < 0.0022$. *C*, Schwann cell proliferation is decreased at both 48 and 72 h in GRD transduced cells compared with Null. ***, $p < 0.0005$; ****, $p < 0.0001$. *GAPDH*, glyceraldehyde-3-phosphate dehydrogenase. *Kda*, kilodaltons.

In addition to Western blotting analysis, proliferation experiments were performed to analyze the functional impact of secondary loss of *Rac1*. The proliferation of both WT and DKO DNSCs were reduced compared with *Nf1*$^{-/-}$ DNSCs (Fig. 3*D*). To delineate the impact of RAC1 in an *Nf1* competent genetic background, *Nf1*$^{+/+}$*Rac1*$^{f/f}$ DNSCs were treated with the GFP or Cre-GFP adenovirus, and 48 h after plating, proliferation was measured. Proliferation was decreased in the *Rac1*$^{-/-}$ DNSCs compared with WT (Fig. S3). Conditioned medium was collected and assayed for growth factor expression from all three cell populations; however, no differences were observed between the *Nf1*$^{-/-}$ and DKO samples (Table S3).

Genetic deletion of Rac1 in Nf1-null neural crest–derived cells prevents plexiform neurofibroma formation

To evaluate the biological impact of loss of RAC1 on PN formation, we utilized *PostnCre* to drive recombination of *Nf1* and *Rac1* in neural crest derived Schwann cells (30). *Nf1*$^{flox/flox}$; *PostnCre*$^{+}$ (*Nf1*$^{-/-}$) mice routinely acquire multiple PN on proximal spinal nerve roots by 4–5 months of age and are ubiquitously present by 6–7 months of life (28). *Rac1*$^{flox/flox}$ mice (31) were genetically intercrossed with *Nf1*$^{flox/flox}$;*PostnCre*$^{+}$ mice to generate the *Nf1*$^{flox/flox}$*Rac1*$^{flox/flox}$;*PostnCre*$^{+}$ mice (DKO). Trigeminal nerve was collected from all three genotypes to verify the loss of neurofibromin and/or RAC1 (Fig. 4*A*). All mice were generated on a C57BL/6J and 129SV mixed strain background. Strain analysis indicated ~70% C57BL/6J. Mice from all three genotypes (WT, *Nf1*$^{-/-}$, DKO) were aged for 9 months, and the spinal cord and proximal nerves were harvested to quantify proximal nerve root volume and tumor number by histopathology. As anticipated, multiple large plexiform neurofibromas were observed in *Nf1*$^{-/-}$ mice with 100% penetrance. Average proximal nerve root volume in WT mice at 9 months of age was 0.52 ± 0.24 mm^3 compared with *Nf1*$^{-/-}$ 1.34 ± 0.91 mm^3 (Fig. 4*B*). Furthermore, proximal nerve root volume in DKO mice at 9 months of age was 0.67 ± 0.31 mm^3 compared with *Nf1*$^{-/-}$ mice 1.34 ± 0.91 mm^3 (Fig. 4*B*). The average proximal nerve root volume in DKO mice at 9 months of age was similar to WT (*ns*, Fig. 4*B*). Strikingly, no tumors were observed in the DKO group compared with the *Nf1*$^{-/-}$ mice that averaged 20 PN per mouse (Fig. 4*C*). DKO mice had a smaller body size with decreased mobility observed in 30% of the mice, which has been previously reported to be caused by impaired nerve myelination caused by genetic ablation of *Rac1* (22). Heterozygous loss of *Rac1* was insufficient to significantly decrease proximal nerve root volume or tumor number compared with *Nf1*$^{-/-}$ mice (data not shown).

Evaluation of hematoxylin and eosin (H&E)–stained nerve sections further revealed stark differences in nerve architecture between mouse genotypes. Compared with *Nf1*$^{-/-}$ nerves, which were disrupted and hyperplastic, DKO mice demonstrated reduced cellularity and linear arrangement of Schwann cell similar to WT controls (Fig. 4*D*). Additionally, Masson's trichrome staining of *Nf1*$^{-/-}$ nerves showed large collagen deposits (another hallmark feature of PN), which were not present in WT or DKO tissues (Fig. 4*D*). Collectively, these findings demonstrate a genetic requirement for *Rac1* in plexiform neurofibroma tumor formation *in vivo*.

Discussion

A kinome and Rho GTPase screen identified RAC1 as a novel target to ameliorate PN. Genetic disruption of *RAC1* (*Rac1*) abrogated RAS-mediated cellular and biochemical gain-in-functions in human and murine Schwann cells harboring loss of the *NF1* (*Nf1*) tumor suppressor gene. Here, we show that

biallelic loss of *Rac1* in neural crest–derived cells completely prevented PN tumorigenesis in *Nf1*$^{flox/flox}$;*PostnCre*$^{+}$ mice.

Nearly 30% of all human cancers contain RAS-activating mutations (32). These mutations either reduce extrinsically the ability of the GAP to hydrolyze GTP to GDP or reduce the intrinsic rate of GTP hydrolysis, leading to increased RAS activation, proliferation, and growth signaling. Unlike oncogenic RAS mutations, patients with NF1 have normal RAS but are

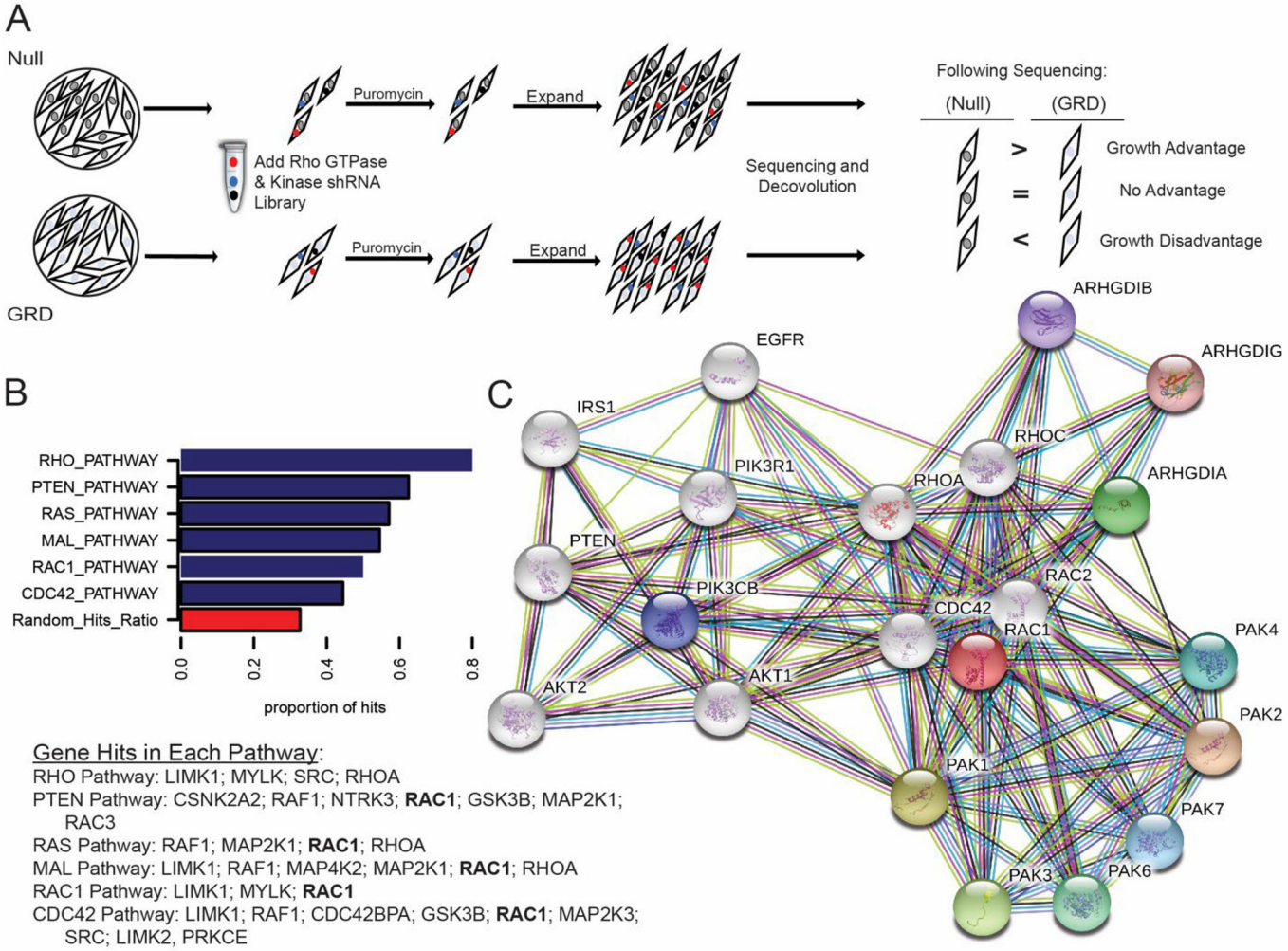

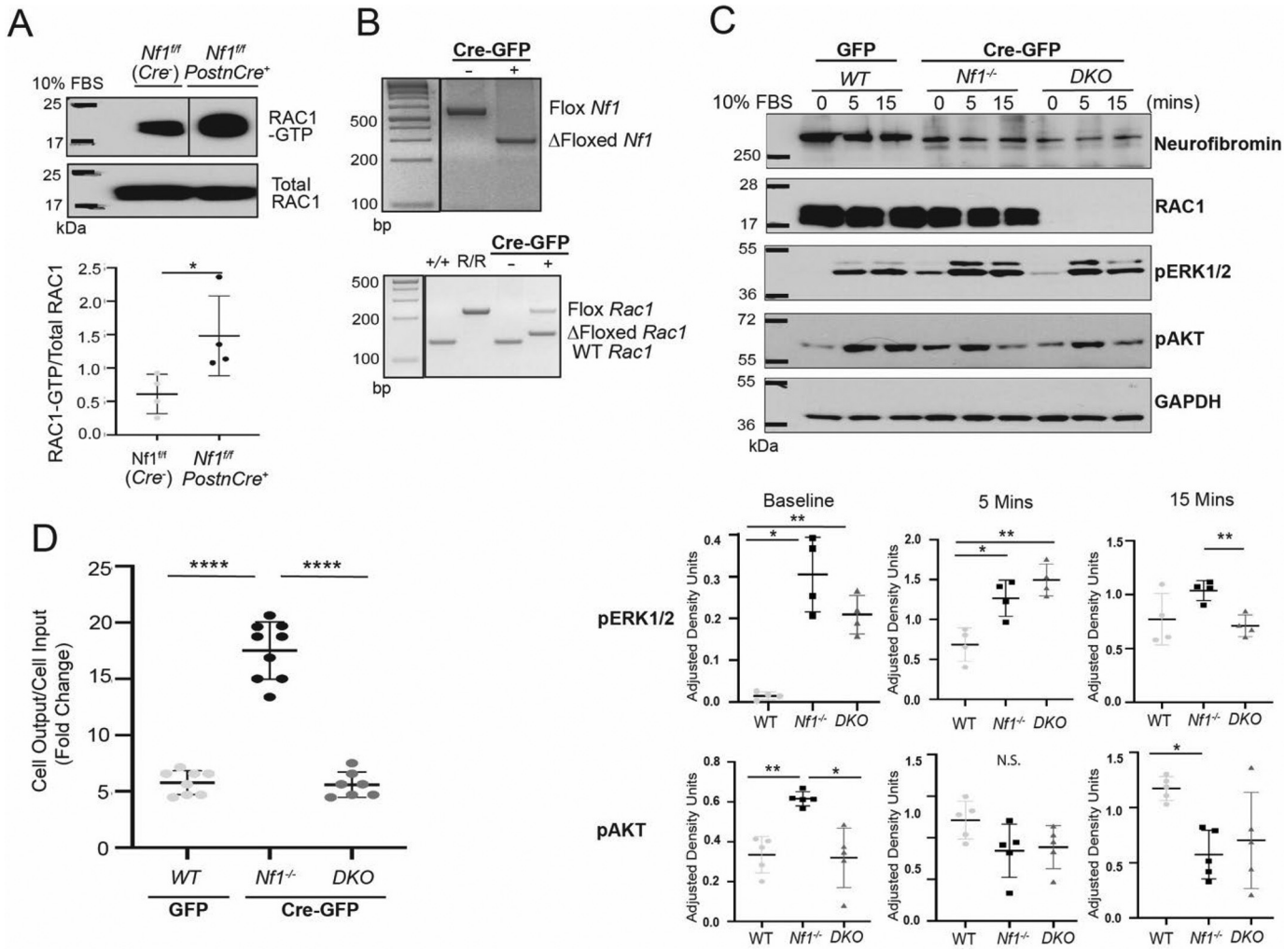

Figure 3. Genetic ablation of *Rac1* ameliorates biochemical and cellular gain in functions in *Nf1*$^{-/-}$ dorsal root ganglion/ DNSCs. *A*, hyperactive RAC1-GTP is observed in the trigeminal nerve of *Nf1*$^{f/f}$;*PostnCre*$^{+}$ (*Nf1*$^{-/-}$) compared with their *Nf1*$^{f/f}$;*PostnCre*$^{-}$ (WT) littermates. *B*, *Nf1*$^{f/f}$ and *Nf1*$^{f/f}$;*Rac1*$^{f/f}$;*PostnCre*$^{-}$ DNSCs were isolated and cultured. Following expansion, the cells were transiently infected with a GFP-Cre adenovirus to delete the floxed alleles or GFP adenovirus as a control. PCR validated Cre-mediated recombination of *Nf1* and *Rac1*. *C*, Western blotting of *Nf1*$^{-/-}$ and DKO DNSCs showed hyperactive phospho-ERK1/2 at baseline and 5 min after stimulation compared with WT. *, $p < 0.05$; **, $p < 0.01$. DKO DNSCs exhibited decreased pERK1/2 at 15 min after stimulation with 10% FBS in DMEM compared with *Nf1*$^{-/-}$ DNSCs. **, $p < 0.01$. *Nf1*$^{-/-}$ DNSCs exhibited increased phospho-AKT activation at baseline compared with WT and DKO DNSCs. **, $p < 0.01$; *, $p < 0.05$. There was no significant difference between any of the groups at 5 min after stimulation. WT DNSCs had increased activation of phospho-AKT (*pAKT*) at 15 min compared with the *Nf1*$^{-/-}$ DNSCs. *, $p < 0.05$. *D*, the proliferative capacity of WT, *Nf1*$^{-/-}$, and DKO DNSCs was evaluated following adenovirus transduction. WT and DKO DNSCs had decreased proliferation compared with *Nf1*$^{-/-}$. ****, $p < 0.0001$ for each pair. There was no difference in proliferation observed between WT and DKO ($p = 0.9971$). *GAPDH*, glyceraldehyde-3-phosphate dehydrogenase. *AKT*, protein kinase B, *Kda*, kilodaltons.

missing neurofibromin, leading to RAS hyperactivation. Mechanism-based therapies to directly target core components of the RAS–GAP molecular switch have been exceedingly difficult to develop (33, 34). GTP is abundant in cells, and RAS binds guanine nucleotides with very high affinity (33). Thus, inhibition of RAS GTP binding would require compounds with very high binding affinities, well above those of other FDA-approved small molecule inhibitors. Alternative approaches to enhance GTP hydrolysis have also proved challenging because of the structurally constrained interface between the phosphate-binding loop of RAS and GAPs (8, 32). Thus, therapeutic strategies targeting downstream RAS effectors hold promise in the treatment of *NF1* and other RAS-driven cancers.

Figure 2. RAC1 knockdown reduces phospho-ERK1/2 signaling and proliferation in *NF1*$^{-/-}$ (Null) immortalized human Schwann cells. *A*, schematic of the experimental workflow for the pooled human kinase and Rho-GTPase shRNA library screen. *B*, pathway analysis of the deconvoluted shRNA library screen hairpins following sequencing. RAC1 was observed in multiple pathways that were above the random hits ratio, indicating a strong candidate. *C*, STRING analysis links RAC1 with many downstream effectors of RAS. *D*, hyperactive phospho-ERK1/2 signaling is decreased at 15 and 30 min after stimulation with 10% FBS in DMEM following shRNA knockdown of RAC1 in patient-derived Null cells. ***, $p < 0.001$; ***, $p < 0.001$. *E*, shRNA knockdown of RAC1 modulates proliferation of Null Schwann cells. At 48 h, proliferation of GRD and Null + RAC1 shRNA transduced Schwann cells was significantly decreased compared with Null. ****, $p < 0.0001$; ***, $p < 0.0005$. There is also a slight decrease in the proliferation of GRD Schwann cells compared with those transduced with Null + RAC1 shRNA. *, $p < 0.05$. At 72 h, proliferation of GRD and Null + RAC1 shRNA transduced Schwann cells were both significantly decreased compared with Null. ****, $p < 0.0001$. There was no difference in proliferation between the GRD and the Null + RAC1 shRNA transduced Schwann cells. *GAPDH*, glyceraldehyde-3-phosphate dehydrogenase.

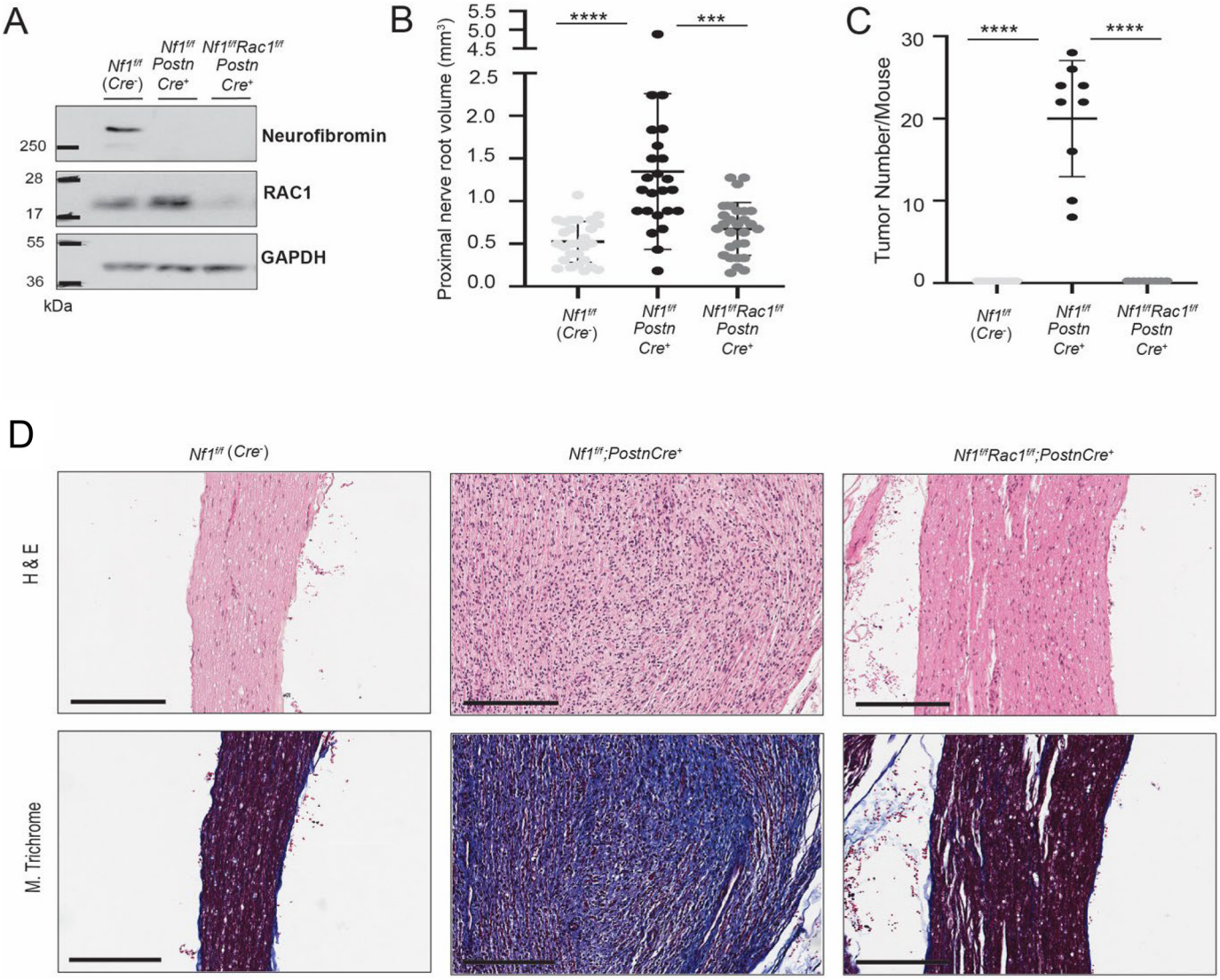

Figure 4. Knockout of *Rac1* in neural crest derived Schwann cells prevents plexiform neurofibroma formation in a murine model of NF1. *A*, Western blotting analysis of trigeminal nerve validating the absence of RAC1 and Neurofibromin in the $Nf1^{flox/flox}$ and $Nf1^{flox/flox}$;$Rac1^{flox/flox}$ PostnCre mouse models. *B*, proximal nerve root volume in 8–9-month-old $Nf1^{flox/flox}$;$PostnCre^{-}$, $Nf1^{flox/flox}$;$PostnCre^{+}$, and $Nf1^{flox/flox}$;$Rac1^{flox/flox}$;$PostnCre^{-}$ (WT, $Nf1^{-/-}$, and DKO, respectively) mice. Nerve size between WT and $Nf1^{-/-}$ was significantly decreased. ****, $p < 0.0001$. Nerve size between DKO and $Nf1^{-/-}$ was also significantly reduced. ****, $p < 0.0001$. There was no significant difference between WT and DKO. *C*, plexiform neurofibroma tumors were identified by histopathological examination of nerve tissues microdissected from 8–9-month-old WT, $Nf1^{-/-}$, and DKO mice. Zero tumors were observed in both the WT and DKO cohorts. $Nf1^{-/-}$ tumor number was significantly different to both the WT and DKO. ****, $p < 0.0001$ between each pair. *D*, representative H&E–stained sections of the proximal nerve trees demonstrate changes in nerve microarchitecture between the three genotypes of mice (WT, $Nf1^{-/-}$, and DKO). Masson's trichrome–stained sections show extracellular matrix collagen. *Scale bars*, 200 μm. *GAPDH*, glyceraldehyde-3-phosphate dehydrogenase.

Novel kinase-targeting drug candidates have shown recent success in ameliorating the growth of PN in patients including MEK (selumetinib (13)) and ABL, c-kit, and platelet-derived growth factor receptor (imatinib mesylate) (12). Even with these successes, a significant subset of patients do not respond to existing therapies. Moreover, no complete responses have been observed to date, and tumors often regrow when drug therapy is discontinued. Thus, additional pharmacotherapies are needed to improve treatment outcomes for NF1 patients with PN.

The RNAi Consortium (TRC) was developed to create library of custom RNAi constructs targeting 15,000 human and murine genes (27). First phase (TRC1) constructs were developed from the initial RNAi constructs with various knockdown transduction efficiency. Second generation, TRC2 constructs were validated for high knockdown efficiency and provide a standard for RNAi experiments. Three to five TRC1 and TRC2 hairpin constructs per gene were employed to ensure target knockdown. Our shRNA screen identified multiple genes including *RAC1*, which selectively decreased the growth of $NF1^{-/-}$ human Schwann cells. Furthermore, protein–protein interaction network analysis implicates RAC1 as a unifying modulator of potential targets identified across a range of pathways.

Rho family GTPases have complex regulation and redundancy in signaling pathways given their many essential roles in coordinating cellular functions. Additionally, multiple GEFs and GAPS are recognized to spatiotemporally modulate Rho GTPase signaling (35). RAC1 is a key node downstream of RAS

with cross-talk observed in RAS–RAF–MEK-ERK signaling. Hyperactivation of RAC1 has been reported in human cancers through a variety of mechanisms, including mutation of RAC1 itself, impaired degradation of RAC1, and increased activation of upstream effectors (23, 36).

Genetically engineered mouse models have proven tremendously valuable in elucidating mechanisms of NF1 disease pathogenesis and evaluating novel treatments and proofs of concept (28, 29, 37–42). Tissue-specific models driven by Cre-Lox recombination have been essential for overcoming the embryonic lethality associated with germline, biallelic *Nf1* loss caused by abnormal cardiac development by E13.5 (43, 44). Similarly, RAC1 is ubiquitously expressed and essential for early embryonic development, leading to lethality by E8 (45). Recently, an elegant study identified the PN cell of origin in the nerve roots of E13.5 embryos (29). Here, we generated mice harboring conditional biallelic inactivation of *Nf1* and *Rac1* ($Nf1^{flox/flox}Rac1^{flox/flox}$;$PostnCre^{+}$) in neural crest Schwann cell precursors driven at E10 by PostnCre (30). $Nf1^{flox/flox}$;$PostnCre^{+}$ mice develop multiple PN with 100% penetrance by 6 months of life (28). In the present study, all cohorts were evaluated at 9 months of life, suggesting a total absence of PN in $Nf1^{flox/flox}Rac1^{flox/flox}$;$PostnCre^{+}$ mice rather than merely a delay in in tumor formation.

We questioned whether there may be a cell extrinsic effect of *Rac1* ablation on disrupting paracrine signaling between the tumorigenic Schwann cells and lineages in the microenvironment. Prior work has shown a key role of cytokines in the recruitment of tumor promoting immune cells into the PN microenvironment (37, 46, 47). We quantified 30 growth factors in conditioned medium, including stem cell factor, which via its receptor c-kit is key to tumor initiation (37). We found that disruption of *Rac1* in *Nf1*-deficient DNSCs did not alter growth factor secretion (Table S3).

In summary, we show here that genetic disruption of *RAC1* (*Rac1*) in $NF1^{-/-}$ ($Nf1^{-/-}$) Schwann cells strongly modulates proliferation and pERK signaling. Pharmacological strategies to inhibit RAC1 have focused predominantly on disrupting RAC1/GEF interactions. This has been challenging because RAC1, like RAS, has a small binding pocket (48). Presently, a RAC1 targeted therapeutic is not clinically available (48), although preclinical molecules such as EHop-016, a Rac1 and Rac3 inhibitor utilized in this study, may provide a platform for future drug development. The preclinical studies outlined here provide a proof of concept for the potential role of RAC1 inhibitors in modulating the genesis and growth of Ras-dependent NF1 tumors.

Experimental procedures

Human paired cell line

$NF1^{-/-}$ patient-derived cell line 05.5 was generously donated by M. R. Wallace. NF1 GRD:T2A GFP lentiviral particles were generated by Vector Builder using a previously published construct (3, 4). The GRD construct sequence and vector map are included in Fig. S1 (*A* and *B*), respectively. The 05.5 cell line was transduced overnight with either the NF1 GRD:T2A GFP (GRD) lentivirus or a scramble shRNA construct with a GFP reporter (Null). 72 h later, GFP^{+} cells were sorted on a FACS Aria (BD) and expanded in 10% fetal bovine serum in DMEM with 1% GlutaMAX (Gibco) and 1% penicillin/streptomycin (Gibco) medium for validation and future use.

shRNA library screen

The human kinase pool of lentiviral particles and the combined shRNA library include 3200 shRNA hairpins targeting 501 genes and included nontargeting controls (CSTVRS-07191316MN; Sigma) and a pooled library of Rho-GTPases lentiviral particles (Table S1; Sigma). There were three to five clones on average per target, depending on the number of clones that were validated for knockdown efficiency.

2×10^4 cells/well of each GRD and Null cell line were plated in a tissue culture–coated 24-well dish and treated with puromycin (0, 0.5, 0.75, 1, 1.5, 2, 4, or 5 μg/ml) to determine the kill curve. 100% cell death was observed in both cell lines with 1 μg/ml puromycin at 72 h post-treatment. 5×10^6 cells were plated in 25-cm^3 dishes, and 2.5×10^6 transduction units from the pool of shRNAs against human kinases and Rho-GTPases were added overnight to ensure that cells were transduced with 0 or 1 shRNA. The following morning, fresh medium containing 1 μg/ml puromycin was added and replaced after 48 h. Following 72 h of puromycin selection, with verification of 100% cell death in the nontransduced plates, the medium was replaced with standard culture medium, and the cells were allowed to grow for 14 days. The cells were passaged upon reaching ~85% confluence. 10×10^6 cells from each technical replicate ($n = 3$ per cell line) were sent to Sigma for deconvolution and 1000 × coverage sequencing.

We utilized edgeR to identify the hits with a significantly lower observation rate in the $NF1^{-/-}$ cells *versus* GRD (49). In total, we identified 111 clones that were selectively depleted in $NF1^{-/-}$ (Null) Schwann cells as compared with the GRD normalized controls with a $\log_2$ fold change of <-2 and adjusted p values of <0.1. The random hits ratio was determined by the total number of genes included in the experiment found in at least one pathway with a significant copy number change divided by the total number of genes found in at least one pathway.

Hits were defined as those genes in which at least 20% of all respective hairpins targeting that gene were significantly decreased according to the following criteria: 1) a log fold change of <-2 when comparing Null cells *versus* GRD, and 2) adjusted p values below the false discovery rate of <0.1. Pathway enrichment analysis was conducted by using a hypergeometric test of identified possible target genes against 1329 MsigDB v6 canonical pathways (50), with using the 536 total screened genes as the background and $p < 0.05$ as the cutoff for statistical significance. Full sequencing data are available on ArrayExpress (E-MTAB-8398), and the read counts for each clone and biological replicate are provided in Table S2.

Rac1 shRNA

1×10^6 Null cells were plated in three 10-cm tissue culture–coated dishes, and 0.75×10^6 Rac1shRNA (Sigma, TRCN0000055189) lentiviral particles were added to two dishes overnight. The additional dish of cells was left

nontransduced to verify puromycin selection. The following morning, fresh culture medium containing 1 μg/ml puromycin was added to the plates and replaced after 48 h. Following 72 h of puromycin selection, with verification of 100% cell death in the nontransduced plates, medium was replaced with standard culture media, and the cells were expanded for subsequent experiments.

Western blotting

Whole cell lysates were generated from equivalent number of cells, and isolated proteins were fractionated using NuPAGE 4–12% Bis-Tris gels (catalog no. NP0322BOX, Invitrogen) and electrotransferred to polyvinylidene difluoride membranes. Immunoblots were carried out using antibodies to neurofibromin (catalog no. SC-67, Santa Cruz), phospho-ERK1/2 (catalog no. 9101, Cell Signaling Technology), phospho-AKT (catalog no. 4060, Cell Signaling Technology), RAS (catalog no. 05-516, Millepore), RAC1 (catalog no. 05-389, Millepore), and glyceraldehyde-3-phosphate dehydrogenase (catalog no. CST-5174, Cell Signaling Technology). After incubation with the appropriate horseradish peroxidase–conjugated secondary antibodies (anti-rabbit (catalog no. NA934V, GE Healthcare) and anti-mouse (catalog no. NA931, GE Healthcare)), signals were detected with either West Pico PLUS or West Dura horseradish peroxidase substrates (Thermo Scientific) and developed on film. Western blots were performed in three to four independent experiments and analyzed statistically as described below.

Dorsal root ganglia/DNSC culture

DNSC cultures were performed as previously described (29). Briefly, $Nf1^{flox/flox}$;$PostnCre^{-}$ and $Nf1^{flox/flox}Rac1^{flox/flox}$;$PostnCre^{-}$ breeders were established for timed pregnancy experiments. The mice were placed together for 1 night and checked for pregnancy at E13.5. Pregnant mothers were euthanized with embryos collected and dissected for nerve roots. Nerve roots from each embryo were digested in collagenase and plated in complete serum-free medium on ultra low adherent plates to become neurospheres (29). Mature DNSCs were cultured on plates precoated with 10 μg/ml fibronectin. Upon confluency, DNSCs were transduced with 5 μl of high titer Cre-eGFP adenovirus (Ad5CMVCre-eGFP high titer, Indiana University Viral Vector Core) or 5 μl of high titer eGFP adenovirus (Ad5CMVeGFP high titer, University of Iowa Viral Vector Core) for 3 h. Transduction was performed up to three times to ensure efficient Cre-mediated recombination and validated via PCR. Four independent experiments were performed on harvested embryos.

Proliferation assay

0.5×10^5 immortalized Schwann cells or murine primary DNSCs were plated in 12-well plates, and the cells were trypsinized at either 48 or 72 h and counted using a hemocytometer and 0.5% trypan blue. For RAC1 inhibitor experiments, 0.4×10^4 immortalized Schwann cells were plated, and the cells were trypsinized at either 24 or 48 h after adding 6 μM EHop-016 (Selleck Chemicals). Proliferation assays were performed in three independent experiments and analyzed statistically as described below.

Ras immunoprecipitation assay

1×10^6 cells were plated on tissue culture–coated 10-cm dishes 48 h before assay. The cells were starved in DMEM + 1% penicillin/streptomycin (Gibco) for 18 h before stimulation. The cells were stimulated with 10% fetal bovine serum in DMEM with 1% GlutaMAX (Gibco) and 1% penicillin/streptomycin (Gibco) medium, and the Ras activation assay (nonradioactive) was performed per protocol (catalog no. 17-218, EMD Millipore). Ras-IP was performed in three independent experiments and analyzed statistically as described below.

Rac1 immunoprecipitation assay

Trigeminal nerves were isolated from $Nf1^{flox/flox}$; $PostnCre^{+}$ (WT) and $Nf1^{flox/flox}$; $PostnCre^{-}$ ($Nf1^{-/-}$) mice and were minced in lysis buffer and sonicated followed by centrifugation at 13,000 rpm for 5 min at 4 °C. Supernatant was transferred to a new microcentrifuge tube, and the Rac1 activation assay (nonradioactive) was performed per protocol (catalog no. 17-283, EMD Millipore). Rac1-IP was performed in three independent experiments and analyzed statistically as described below.

Mouse growth factor array

1×10^6 $Nf1^{flox/flox}$ and $Nf1^{flox/flox}Rac1^{flox/flox}$ DNSCs after adenovirus transduction were seeded on precoated 10-cm^3 plates with 10 μg/ml fibronectin and upon confluency were starved in basal DNSC media without growth factors (29). Conditioned medium was harvested after 18 h and centrifuged to eliminate any cellular debris. The cells were harvested, and a bicinchoninic acid assay was performed to normalize the conditioned media concentrations. Conditioned medium was assessed without delay in mouse growth factor array 3 (catalog no. AAM-GF-3, Ray Biotech) as per protocol. The assay was performed in duplicate in two independent experiments for four total replicates per genotype.

Animals

The WT and $Nf1^{flox/flox}$;$PostnCre^{+}$ mice utilized in these studies have been previously described (28). $Rac1^{flox/flox}$ *mice* (129SV background, JAX 005550) (51) were bred with $Nf1^{flox/flox}$;$PostnCre^{+}$ mice to generate $Nf1^{flox/flox}$;$Rac1^{flox/+}$;$PostnCre^{+}$ and $Nf1^{flox/flox}Rac1^{flox/flox}$;$PostnCre^{+}$ mice. The genotypes were confirmed by PCR. The WT, *Nf1* floxed, and recombination bands were detected using the following primers: P1, 5′-AATGTGAAATTGGTGTCGAGTAAGGTAACCAC-3′; P2, 5′-TTAAGAGCATCTGCTGCTCTTAGAGGGAA-3′; and P3, 5′-TCAGACTGATTGTTGTACCTGATGGTTGTACC-3′. *Rac1* WT, floxed, and recombination bands were detected using the following primers: P1, 5′-GATGCTTCTAGGGGTGAGCC-3′; P2, 5′-TCCAATCTGTGCTGCCCATC-3′; and P3, 5′-CAGAGCTCGAATCCAGAAACTAGTA-3′. *PostnCre* was detected using the following primers: forward, 5′-ATGTTTAGCTGGCCCAAATG-3′; and reverse, 5′-CGACCACTACCAGCAGAACA-

3′. All protocols were approved by the Institutional Animal Care and Use Committee at Indiana University School of Medicine.

Microdissection of nerve tree and measurement of proximal nerve volume

Immediately following euthanasia, the mice were perfused and fixed in 10% neutral buffered formalin. Following decalcification, the lumbosacral spinal nerve tree was then isolated under a dissection microscope. The volume of proximal peripheral nerves was determined using calipers to measure the lengths and widths of the dissected tumors (or the equivalent region in the absence of a tumor) in maximal dimension. The volume was then approximated using the formula for the volume of a spheroid = $0.52 \times (\text{width})^2 \times \text{length}$.

Histological analysis

Following volumetric proximal nerve measurements, the nerve trees were dehydrated with graded alcohols, cleared with xylenes, infiltrated with molten paraffin, and embedded in paraffin blocks. 5-μm-thick sections were cut on a Leica rotary microtome and stained with H&E. Tissue sections were also stained with Masson's trichrome to identify collagen. Whole slide images were acquired on an Aperio ScanScope CS.

Statistics

Statistical analyses were performed with GraphPad Prism 7.0 software (GraphPad, La Jolla, CA). Analysis of variance and Student's *t* tests with post hoc correction for multiple comparisons were used to evaluate for statistically significant differences between samples as described in detail within the figure legends.

Data availability

All data are contained within the manuscript. Raw sequencing data (FASTQ files) for the human kinase and Rho-GTPase shRNA library screen are available on ArrayExpress (E-MTAB-8398).

Author contributions—J. A. M., S.-J. P., A. E. S., L. J., E. H., D. K. M., J. Y., W. K. B., G. S., S. C., S. D. R., and D. W. C. conceptualization; J. A. M., L. J., E. H., S. C., and D. W. C. resources; J. A. M., S.-J. P., Y. H., L. J., E. H., M. J. R., D. K. M., J. Y., W. K. B., G. S., S. C., C. Z., S. D. R., and D. W. C. data curation; J. A. M., S.-J. P., A. E. S., Y. H., L. J., E. H., M. J. R., D. K. M.J. Y., W. K. B., G. S., S. C., CZ, and D. W. C. formal analysis; J. A. M., S.-J. P., A. E. S., L. J., E. H., D. K. M., W. K. B., G. S., S. C., C. Z., S. D. R., and D. W. C. supervision; J. A. M., L. J., E. H., S. C., and D. W. C. funding acquisition; J. A. M., S.-J. P., A. E. S., D. K. M., W. K. B., and CZ validation; J. A. M., S.-J. P., E. H., M. J. R., and J. Y. investigation; J. A. M., S.-J. P., A. E. S., Y. H., L. J., E. H., M. J. R., M. A.-S., W. K. B., G. S., S. C., CZ, S. D. R., and D. W. C. methodology; J. A. M., S.-J. P., L. J., E. H., D. K. M., W. K. B., G. S., S. C., S. D. R., and D. W. C. writing-original draft; J. A. M., S.-J. P., A. E. S., L. J., E. H., G. S., S. C., S. D. R., and D. W. C. writing-review and editing; A. E. S., Y. H., L. J., E. H., and M. J. R. visualization; D. K. M., W. K. B., G. S., and S. D. R. project administration.

Funding and additional information—This work was supported by a Developmental and Hyperactive Ras Tumor SPORE funded through NCI, National Institutes of Health Grant U54-CA196519-04 and NCI/NINDS, National Institutes of Health Grant R01NS104489-02. Julie Mund is a predoctoral fellow supported by Institutional National Research Service Award T32 through Award 5T32DK007519-34. Steven Rhodes is a fellow in the Pediatric Scientist Development Program supported by Award K12-HD000850-35 from the Eunice Kennedy Shriver National Institute of Child Health and Human Development.. The content is solely the responsibility of the authors and does not necessarily represent the official views of the National Institutes of Health.

Conflict of interest—The authors declare that they have no conflicts of interest with the contents of this article.

Abbreviations—The abbreviations used are: NF1, neurofibromatosis type 1; GAP, GTPase-activating protein; PN, plexiform neurofibroma; ERK, extracellular signal–regulated kinase; GRD, GAP-related domain; IP, immunoprecipitation; DNSC, dorsal nerve root neurosphere cell; E*n*, embryonic day n; H&E, hematoxylin and eosin; MEK, mitogen-activated protein kinase kinase; TRC, The RNAi Consortium; DMEM, Dulbecco's modified Eagle's medium; FBS, fetal bovine serum; GTP, guanosine triphosphate.

References

1. Wallace, M. R., Marchuk, D. A., Andersen, L. B., Letcher, R., Odeh, H. M., Saulino, A. M., Fountain, J. W., Brereton, A., Nicholson, J., and Mitchell, A. L. (1990) Type 1 neurofibromatosis gene: identification of a large transcript disrupted in three NF1 patients. *Science* **249,** 181–186 CrossRef Medline
2. Viskochil, D., Buchberg, A. M., Xu, G., Cawthon, R. M., Stevens, J., Wolff, R. K., Culver, M., Carey, J. C., Copeland, N. G., Jenkins, N. A., White, R., and O'Connell, P. (1990) Deletions and a translocation interrupt a cloned gene at the neurofibromatosis type 1 locus. *Cell* **62,** 187–192 CrossRef Medline
3. Hiatt, K. K., Ingram, D. A., Zhang, Y., Bollag, G., and Clapp, D. W. (2001) Neurofibromin GTPase-activating protein-related domains restore normal growth in $Nf1^{-/-}$ cells. *J. Biol. Chem.* **276,** 7240–7245 CrossRef Medline
4. Martin, G. A., Viskochil, D., Bollag, G., McCabe, P. C., Crosier, W. J., Haubruck, H., Conroy, L., Clark, R., O'Connell, P., and Cawthon, R. M. (1990) The GAP-related domain of the neurofibromatosis type 1 gene product interacts with ras p21. *Cell* **63,** 843–849 CrossRef Medline
5. Stephen, A. G., Esposito, D., Bagni, R. K., and McCormick, F. (2014) Dragging ras back in the ring. *Cancer Cell* **25,** 272–281 CrossRef Medline
6. Birnbaum, R. A., O'Marcaigh, A., Wardak, Z., Zhang, Y. Y., Dranoff, G., Jacks, T., Clapp, D. W., and Shannon, K. M. (2000) Nf1 and Gmcsf interact in myeloid leukemogenesis. *Mol. Cell* **5,** 189–195 CrossRef Medline
7. DeClue, J. E., Heffelfinger, S., Benvenuto, G., Ling, B., Li, S., Rui, W., Vass, W. C., Viskochil, D., and Ratner, N. (2000) Epidermal growth factor receptor expression in neurofibromatosis type 1-related tumors and NF1 animal models. *J. Clin. Invest.* **105,** 1233–1241 CrossRef Medline
8. Simanshu, D. K., Nissley, D. V., and McCormick, F. (2017) RAS proteins and their regulators in human disease. *Cell* **170,** 17–33 CrossRef Medline
9. Staser, K., Yang, F. C., and Clapp, D. W. (2012) Pathogenesis of plexiform neurofibroma: tumor-stromal/hematopoietic interactions in tumor progression. *Annu. Rev. Pathol.* **7,** 469–495 CrossRef Medline
10. Gutmann, D. H., Blakeley, J. O., Korf, B. R., and Packer, R. J. (2013) Optimizing biologically targeted clinical trials for neurofibromatosis. *Expert Opin. Investig. Drugs* **22,** 443–462 CrossRef Medline
11. Canavese, F., and Krajbich, J. I. (2011) Resection of plexiform neurofibromas in children with neurofibromatosis type 1. *J. Pediatr. Orthop.* **31,** 303–311 CrossRef Medline

12. Robertson, K. A., Nalepa, G., Yang, F. C., Bowers, D. C., Ho, C. Y., Hutchins, G. D., Croop, J. M., Vik, T. A., Denne, S. C., Parada, L. F., Hingtgen, C. M., Walsh, L. E., Yu, M., Pradhan, K. R., Edwards-Brown, M. K., *et al.* (2012) Imatinib mesylate for plexiform neurofibromas in patients with neurofibromatosis type 1: a phase 2 trial. *Lancet Oncol.* **13,** 1218–1224 CrossRef Medline
13. Dombi, E., Baldwin, A., Marcus, L. J., Fisher, M. J., Weiss, B., Kim, A., Whitcomb, P., Martin, S., Aschbacher-Smith, L. E., Rizvi, T. A., Wu, J., Ershler, R., Wolters, P., Therrien, J., Glod, J., *et al.* (2016) Activity of selumetinib in neurofibromatosis type 1–related plexiform neurofibromas. *N. Engl. J. Med.* **375,** 2550–2560 CrossRef Medline
14. Ingram, D. A., Hiatt, K., King, A. J., Fisher, L., Shivakumar, R., Derstine, C., Wenning, M. J., Diaz, B., Travers, J. B., Hood, A., Marshall, M., Williams, D. A., and Clapp, D. W. (2001) Hyperactivation of $p21^{ras}$ and the hematopoietic-specific Rho GTPase, Rac2, cooperate to alter the proliferation of neurofibromin-deficient mast cells *in vivo* and *in vitro*. *J. Exp. Med.* **194,** 57–69 CrossRef Medline
15. Bosco, E. E., Mulloy, J. C., and Zheng, Y. (2009) Rac1 GTPase: a "Rac" of all trades. *Cell Mol. Life Sci.* **66,** 370–374 CrossRef Medline
16. Ridley, A. J., Paterson, H. F., Johnston, C. L., Diekmann, D., and Hall, A. (1992) The small GTP-binding protein rac regulates growth factor-induced membrane ruffling. *Cell* **70,** 401–410 CrossRef Medline
17. Etienne-Manneville, S., and Hall, A. (2002) Rho GTPases in cell biology. *Nature* **420,** 629–635 CrossRef Medline
18. Hall, A. (2012) Rho family GTPases. *Biochem. Soc Trans* **40,** 1378–1382 CrossRef Medline
19. Nobes, C. D., and Hall, A. (1999) Rho GTPases control polarity, protrusion, and adhesion during cell movement. *J. Cell Biol.* **144,** 1235–1244 CrossRef Medline
20. Cancelas, J. A., Lee, A. W., Prabhakar, R., Stringer, K. F., Zheng, Y., and Williams, D. A. (2005) Rac GTPases differentially integrate signals regulating hematopoietic stem cell localization. *Nat. Med.* **11,** 886–891 CrossRef Medline
21. Jordan, P., Brazão, R., Boavida, M. G., Gespach, C., and Chastre, E. (1999) Cloning of a novel human Rac1b splice variant with increased expression in colorectal tumors. *Oncogene* **18,** 6835–6839 CrossRef Medline
22. Guo, L., Moon, C., Niehaus, K., Zheng, Y., and Ratner, N. (2012) Rac1 controls Schwann cell myelination through cAMP and NF2/merlin. *J. Neurosci.* **32,** 17251–17261 CrossRef Medline
23. Watson, I. R., Li, L., Cabeceiras, P. K., Mahdavi, M., Gutschner, T., Genovese, G., Wang, G., Fang, Z., Tepper, J. M., Stemke-Hale, K., Tsai, K. Y., Davies, M. A., Mills, G. B., and Chin, L. (2014) The RAC1 P29S hotspot mutation in melanoma confers resistance to pharmacological inhibition of RAF. *Cancer Res.* **74,** 4845–4852 CrossRef Medline
24. Wertheimer, E., Gutierrez-Uzquiza, A., Rosemblit, C., Lopez-Haber, C., Sosa, M. S., and Kazanietz, M. G. (2012) Rac signaling in breast cancer: a tale of GEFs and GAPs. *Cell Signal* **24,** 353–362 CrossRef Medline
25. Hein, A. L., Post, C. M., Sheinin, Y. M., Lakshmanan, I., Natarajan, A., Enke, C. A., Batra, S. K., Ouellette, M. M., and Yan, Y. (2016) RAC1 GTPase promotes the survival of breast cancer cells in response to hyper-fractionated radiation treatment. *Oncogene* **35,** 6319–6329 CrossRef Medline
26. Li, H., Chang, L. J., Neubauer, D. R., Muir, D. F., and Wallace, M. R. (2016) Immortalization of human normal and NF1 neurofibroma Schwann cells. *Lab. Invest.* **96,** 1105–1115 CrossRef Medline
27. Yang, X., Boehm, J. S., Yang, X., Salehi-Ashtiani, K., Hao, T., Shen, Y., Lubonja, R., Thomas, S. R., Alkan, O., Bhimdi, T., Green, T. M., Johannessen, C. M., Silver, S. J., Nguyen, C., Murray, R. R., *et al.* (2011) A public genome-scale lentiviral expression library of human ORFs. *Nat. Methods* **8,** 659–661 CrossRef Medline
28. Rhodes, S. D., He, Y., Smith, A., Jiang, L., Lu, Q., Mund, J., Li, X., Bessler, W., Qian, S., Dyer, W., Sandusky, G. E., Horvai, A. E., Armstrong, A. E., and Clapp, D. W. (2019) Cdkn2a (Arf) loss drives NF1-associated atypical neurofibroma and malignant transformation. *Hum. Mol. Genet.* **28,** 2752–2762 CrossRef Medline
29. Chen, Z., Liu, C., Patel, A. J., Liao, C. P., Wang, Y., and Le, L. Q. (2014) Cells of origin in the embryonic nerve roots for NF1-associated plexiform neurofibroma. *Cancer Cell* **26,** 695–706 CrossRef Medline
30. Lindsley, A., Snider, P., Zhou, H., Rogers, R., Wang, J., Olaopa, M., Kruzynska-Frejtag, A., Koushik, S. V., Lilly, B., Burch, J. B., Firulli, A. B., and Conway, S. J. (2007) Identification and characterization of a novel Schwann and outflow tract endocardial cushion lineage-restricted periostin enhancer. *Dev. Biol.* **307,** 340–355 CrossRef Medline
31. Gu, Y., Filippi, M. D., Cancelas, J. A., Siefring, J. E., Williams, E. P., Jasti, A. C., Harris, C. E., Lee, A. W., Prabhakar, R., Atkinson, S. J., Kwiatkowski, D. J., and Williams, D. A. (2003) Hematopoietic cell regulation by Rac1 and Rac2 guanosine triphosphatases. *Science* **302,** 445–449 CrossRef Medline
32. Cox, A. D., Fesik, S. W., Kimmelman, A. C., Luo, J., and Der, C. J. (2014) Drugging the undruggable RAS: mission possible? *Nat. Rev. Drug Discov.* **13,** 828–851 CrossRef Medline
33. Downward, J. (2003) Targeting RAS signalling pathways in cancer therapy. *Nat. Rev. Cancer* **3,** 11–22 CrossRef Medline
34. Malumbres, M., and Barbacid, M. (2003) RAS oncogenes: the first 30 years. *Nat. Rev. Cancer* **3,** 459–465 CrossRef Medline
35. Alvarez, D. E., and Agaisse, H. (2014) A role for the small GTPase Rac1 in vaccinia actin-based motility. *Small GTPases* **5,** e29038 CrossRef Medline
36. Haga, R. B., and Ridley, A. J. (2016) Rho GTPases: Regulation and roles in cancer cell biology. *Small GTPases* **7,** 207–221 CrossRef Medline
37. Yang, F. C., Ingram, D. A., Chen, S., Zhu, Y., Yuan, J., Li, X., Yang, X., Knowles, S., Horn, W., Li, Y., Zhang, S., Yang, Y., Vakili, S. T., Yu, M., Burns, D., *et al.* (2008) Nf1-dependent tumors require a microenvironment containing $Nf1^{+/-}$ and c-kit-dependent bone marrow. *Cell* **135,** 437–448 CrossRef Medline
38. Ferguson, M. J., Rhodes, S. D., Jiang, L., Li, X., Yuan, J., Yang, X., Zhang, S., Vakili, S. T., Territo, P., Hutchins, G., Yang, F. C., Ingram, D. A., Clapp, D. W., and Chen, S. (2016) Preclinical Evidence for the use of sunitinib malate in the treatment of plexiform neurofibromas. *Pediatr. Blood Cancer* **63,** 206–213 CrossRef Medline
39. Watson, A. L., Anderson, L. K., Greeley, A. D., Keng, V. W., Rahrmann, E. P., Halfond, A. L., Powell, N. M., Collins, M. H., Rizvi, T., Moertel, C. L., Ratner, N., and Largaespada, D. A. (2014) Co-targeting the MAPK and PI3K/AKT/mTOR pathways in two genetically engineered mouse models of schwann cell tumors reduces tumor grade and multiplicity. *Oncotarget* **5,** 1502–1514 CrossRef Medline
40. Mayes, D. A., Rizvi, T. A., Cancelas, J. A., Kolasinski, N. T., Ciraolo, G. M., Stemmer-Rachamimov, A. O., and Ratner, N. (2011) Perinatal or adult Nf1 inactivation using tamoxifen-inducible PlpCre each cause neurofibroma formation. *Cancer Res.* **71,** 4675–4685 CrossRef Medline
41. Wu, J., Williams, J. P., Rizvi, T. A., Kordich, J. J., Witte, D., Meijer, D., Stemmer-Rachamimov, A. O., Cancelas, J. A., and Ratner, N. (2008) Plexiform and dermal neurofibromas and pigmentation are caused by Nf1 loss in desert hedgehog-expressing cells. *Cancer Cell* **13,** 105–116 CrossRef Medline
42. Zhu, Y., Ghosh, P., Charnay, P., Burns, D. K., and Parada, L. F. (2002) Neurofibromas in NF1: Schwann cell origin and role of tumor environment. *Science* **296,** 920–922 CrossRef Medline
43. Jacks, T., Shih, T. S., Schmitt, E. M., Bronson, R. T., Bernards, A., and Weinberg, R. A. (1994) Tumour predisposition in mice heterozygous for a targeted mutation in Nf1. *Nat. Genet.* **7,** 353–361 CrossRef Medline
44. Brannan, C. I., Perkins, A. S., Vogel, K. S., Ratner, N., Nordlund, M. L., Reid, S. W., Buchberg, A. M., Jenkins, N. A., Parada, L. F., and Copeland, N. G. (1994) Targeted disruption of the neurofibromatosis type-1 gene leads to developmental abnormalities in heart and various neural crest-derived tissues. *Genes Dev.* **8,** 1019–1029 CrossRef Medline
45. Sugihara, K., Nakatsuji, N., Nakamura, K., Nakao, K., Hashimoto, R., Otani, H., Sakagami, H., Kondo, H., Nozawa, S., Aiba, A., and Katsuki, M. (1998) Rac1 is required for the formation of three germ layers during gastrulation. *Oncogene* **17,** 3427–3433 CrossRef Medline
46. Liao, C. P., Booker, R. C., Brosseau, J. P., Chen, Z., Mo, J., Tchegnon, E., Wang, Y., Clapp, D. W., and Le, L. Q. (2018) Contributions of inflammation and tumor microenvironment to neurofibroma tumorigenesis. *J. Clin. Invest.* **128,** 2848–2861 CrossRef Medline
47. Brosseau, J. P., Liao, C. P., Wang, Y., Ramani, V., Vandergriff, T., Lee, M., Patel, A., Ariizumi, K., and Le, L. Q. (2018) NF1 heterozygosity fosters *de*

novo tumorigenesis but impairs malignant transformation. *Nat. Commun.* **9,** 5014 CrossRef Medline

48. Lin, Y., and Zheng, Y. (2015) Approaches of targeting Rho GTPases in cancer drug discovery. *Expert Opin. Drug Discov.* **10,** 991–1010 CrossRef Medline
49. Dai, Z., Sheridan, J. M., Gearing, L. J., Moore, D. L., Su, S., Wormald, S., Wilcox, S., O'Connor, L., Dickins, R. A., Blewitt, M. E., and Ritchie, M. E. (2014) edgeR: a versatile tool for the analysis of shRNA-seq and CRISPR-Cas9 genetic screens. *F1000Res* **3,** 95 CrossRef Medline
50. Subramanian, A., Tamayo, P., Mootha, V. K., Mukherjee, S., Ebert, B. L., Gillette, M. A., Paulovich, A., Pomeroy, S. L., Golub, T. R., Lander, E. S., and Mesirov, J. P. (2005) Gene set enrichment analysis: a knowledge-based approach for interpreting genome-wide expression profiles. *Proc. Natl. Acad. Sci. U.S.A.* **102,** 15545–15550 CrossRef Medline
51. Glogauer, M., Marchal, C. C., Zhu, F., Worku, A., Clausen, B. E., Foerster, I., Marks, P., Downey, G. P., Dinauer, M., and Kwiatkowski, D. J. (2003) Rac1 deletion in mouse neutrophils has selective effects on neutrophil functions. *J. Immunol.* **170,** 5652–5657 CrossRef Medline